WIDEBAND BURST-BY-BURST ADAPTIVE MODULATION USING REDUCED-COMPLEXITY IN-PHASE/QUADRATURE-PHASE TURBO EQUALIZATION

B. L. Yeap, C. H. Wong and L. Hanzo

Dept. of Electr. and Comp. Sc., Univ. of Southampton, SO17 1BJ, UK.
Tel: +44-2380-593 125, Fax: +44-2380-593 045
Email: lh@ecs.soton.ac.uk
http://www-mobile.ecs.soton.ac.uk

ABSTRACT

The performance of burst-by-burst adaptive modulation is studied in conjunction with reduced complexity turbo equalization over a wideband multi-path Rayleigh fading channel. By employing the reduced complexity turbo equalizer, higher-order modulation modes such as 64-level Quadrature Amplitude Modulation (64-QAM) can be invoked, than upon using the conventional turbo equalizer. The structure of the reduced complexity turbo equalizer was also exploited in order to invoke an iterative least mean square channel estimator. Finally, the performance of the adaptive modulation scheme was compared to that of its constituent modulation modes and a signal-to-noise ratio gain of 1.0dB to 1.5dB was recorded for the throughput range of 0.5 to 2.0 bits/symbol.

I. INTRODUCTION

Adaptive Quadrature Amplitude Modulation (AQAM) [1] is based on a modulation mode switching regime, in which the modulation modes are selected according to the prevalent near-instantaneous channel conditions. When the channel quality is low, lower-order modulation modes are selected, in order to improve the mean Bit Error Rate (BER) performance and similarly, higher-order modulation modes are activated, when the channel quality is favourable, in order to increase the system's average throughput. Recent AQAM-related advances over narrowband channels have been accomplished amongst others by Sampei *et al.* [2] and Goldsmith *et al.* [3]. In a wideband environment, the presence of intersymbol interference (ISI) is combated not only by the employment of AQAM, but also by channel equalization. Hence we utilized the Signal to residual intersymbol Interference plus Noise ratio (SINR) at the output of the channel equalizer - termed as the pseudo-SNR - in order to switch the modulation modes. In this contribution, we will study the performance of AQAM in conjunction with reduced complexity turbo equalization. Previous work by Wong *et al.* [4] has employed the conventional turbo equalizer proposed by Douillard *et al.* [5], in conjunction with AQAM. However, due to the high complexity of the turbo equalizer, the highest-order modulation mode utilised was 16-QAM.

Turbo equalization [5] was first introduced by Douillard *et al.* [5] in 1995 for a rate $R = 0.5$ convolutional coded BPSK system. Specifically, Douillard *et al.* [5] demonstrated that the turbo equalizer was capable of mitigating the effects of Inter-Symbol Interference (ISI), when performing channel equalization and channel decoding jointly and iteratively. The advantages of performing the equalization and decoding jointly were further highlighted by Knickenberg *et al.* [6], who proposed a non-iterative joint equalization and decoding technique based on a supertrellis structure. This technique yielded an optimum performance, but it was restricted to incorporating simple interleavers due to the high complexity incurred by large interleaver arrays. Early turbo equalization investigations using the conventional trellis-based equalizer (CT-EQ) were constrained to applying Binary Phase Shift Keying (BPSK) and Quadrature Phase Shift Keying (QPSK) modulation schemes [7] and to limited Channel Impulse Response (CIR) durations, since the computational complexity incurred by the CT-EQ is dependent on both the maximum CIR duration and on the modulation mode utilised. Hence, turbo equalization research has been focused on developing reduced complexity equalizers, such as the low-complexity linear equalizer proposed by Glavieux *et al.* [8], the reduced complexity Inphase/Quadrature-phase Equalizer (I/Q-EQ) [9] and the Radial Basis Function (RBF) equalizer advocated by Yee *et al.* [10].

Motivated by these trends, the reduced-complexity turbo equalizer of [9] was invoked in conjunction with AQAM [11] in order to improve the Bit Per Symbol (BPS) throughput of the system for a given BER performance.

II. SYSTEM OVERVIEW

The schematic of the system is shown in Figure 1, where the transmitted source bits are convolutionally encoded, interleaved and modulated using a specific AQAM mode selected by the adaptive modulator. The encoder utilized a half-rate Recursive Systematic Convolutional (RSC) code having a constraint length of $K = 5$ and octal generator polynomials of $G0 = 35$ and $G1 = 23$. A random channel interleaver of 12096-bit memory was employed.

The modulated signal $s(t)$ is transmitted over the channel characterised by the CIR $h(t)$ and further corrupted by the zero-mean complex white Gaussian noise $n(t)$ — having a

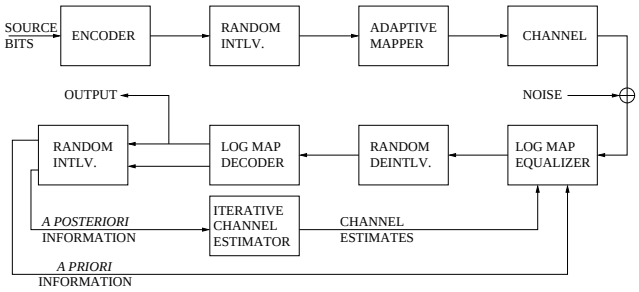

Fig. 1. Schematic of the joint turbo equalization and adaptive modulation system.

variance of $\sigma^2 = N_o/2$, where N_o is the single-sided noise power spectral density — at the receiver in order to yield the received signal $r(t)$. Since the CIR $h(t)$ is complex, consisting of the in-phase component $h_I(t)$ and quadrature-phase component $h_Q(t)$, the resultant received signal $r(t)$ is:

$$\begin{aligned} r(t) &= s(t) * h(t) + n(t) \\ &= [s_I(t) + j s_Q(t)] * [h_I(t) + j h_Q(t)] + n_I(t) + j n_Q(t) \\ &= r_I(t) + j r_Q(t), \end{aligned} \tag{1}$$

where

$$\begin{aligned} r_I(t) &= s_I(t) * h_I(t) - s_Q(t) * h_Q(t) + n_I(t) \\ r_Q(t) &= s_I(t) * h_Q(t) + s_Q(t) * h_I(t) + n_Q(t) \end{aligned} \tag{2}$$

and $s_I(t)$ and $s_Q(t)$ are the I and Q components of the transmitted signal $s(t)$, as illustrated in Figure 2. Furthermore,

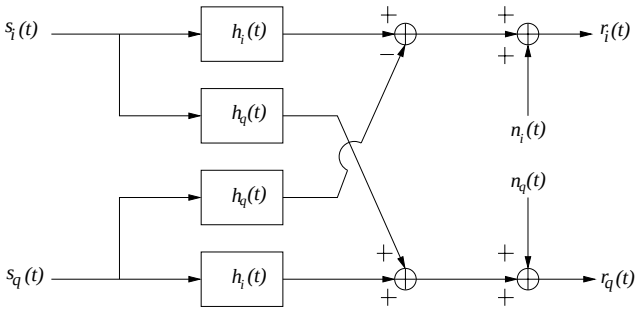

Fig. 2. Model of the complex, dispersive CIR. After transmission over the channel having a complex CIR, the received signal $r(t)$ becomes dependent on the in-phase component $s_I(t)$ and quadrature-phase component $s_Q(t)$ of the transmitted signal, as expressed in Equations 1 and 2.

$n_I(t)$ and $n_Q(t)$ are the quadrature components of the Gaussian noise $n(t)$. Subsequently, the turbo equalizer processes the corrupted received signal, in order to determine the transmitted source bits.

The AQAM mode was selected based on the pseudo-SNR, γ_{dfe}, where the switching methodology can be summarized as follows:

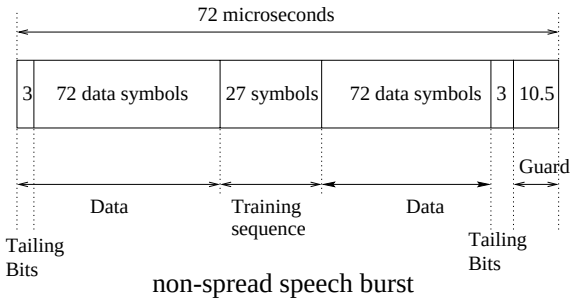

Fig. 3. Transmission burst structure of the FMA1 non-spread speech burst of the FRAMES proposal [15].

$$\text{Modulation Mode} = \begin{cases} \text{NOTX} & \text{if } \gamma_{dfe} < f_1 \\ \text{BPSK} & \text{if } f_1 \le \gamma_{dfe} < f_2 \\ \text{4-QAM} & \text{if } f_2 \le \gamma_{dfe} < f_3 \\ \text{16-QAM} & \text{if } f_3 \le \gamma_{dfe} < f_4 \\ \text{64-QAM} & \text{if } f_4 \le \gamma_{dfe} \end{cases} \tag{3}$$

while $f_n, n = 1...4$ are the pseudo-SNR switching thresholds. In our investigations, the switching thresholds, which are associated with a specific channel impulse response, have been determined following the approach of [12] using Powell's optimization, such that the required target BER was maintained. Accordingly, for low-quality channels the value of the switching thresholds would be higher than the thresholds of high-quality channels, in order to discourage the excessive use of error-sensitive, but high-throughput AQAM modes. Recent research [13, 14] revealed that a higher throughput can be maintained, when the switching thresholds are SNR-dependent, in order to encourage the employment of high-throughput AQAM modes under high channel quality conditions. The NOTX mode is used for temporarily disabling transmissions under severely degraded instantaneous channel conditions.

The transmission burst structure used in this system is the FMA1 non-spread speech burst as specified in the Pan-European FRAMES proposal [15], which is seen in Figure 3. A three-path, symbol-spaced fading channel of equal weights was utilized, where the Rayleigh fading statistics obeyed a normalised Doppler frequency of 3.3615×10^{-5}. At the receiver, the CIR was iteratively estimated using the Least Mean Square (LMS) algorithm [4, 11] with the aid of the training symbols of the transmission burst shown in Figure 3.

III. PRINCIPLES OF IN-PHASE/QUADRATURE-PHASE EQUALIZATION

As shown in Equation 2, the I/Q components of the received signals, namely $r_I(t)$ and $r_Q(t)$, become dependent on $s_I(t)$ and $s_Q(t)$ after convolution with the complex CIR. The cross-correlation between $s_I(t)$ and $s_Q(t)$ in $r_I(t)$ and $r_Q(t)$ is referred to here as **cross-coupling**. As a consequence of the cross-coupling between the transmitted signal's quadrature components, the receiver must consider an

increased number of signal combinations, hence necessitating a high number of equalizer trellis states.

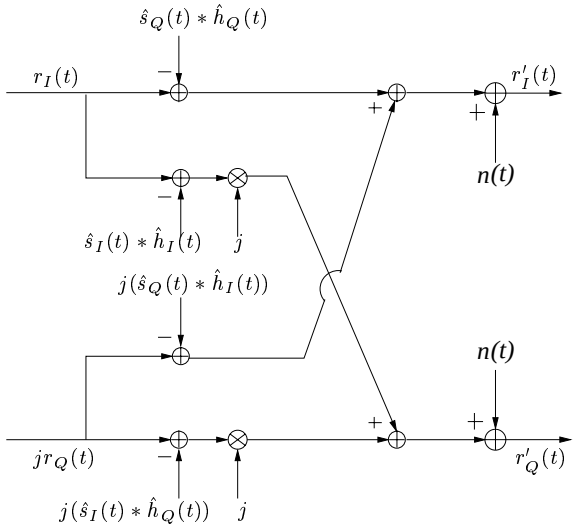

Fig. 4. Removing the dependency of $r_I(t)$ and $r_Q(t)$ on the quadrature components of the transmitted signals, namely $s_I(t)$ and $s_Q(t)$, to give $r'_I(t)$ and $r'_Q(t)$, respectively. In this figure, it is assumed that the CIR estimation is perfect, *i.e.* $\hat{h}_I(t) = h_I(t)$ and $\hat{h}_Q(t) = h_Q(t)$ and that the transmitted signals are known, giving $\hat{s}_I(t) = s_I(t)$ and $\hat{s}_Q(t) = s_Q(t)$. In this case, perfect decoupling is achieved. However, in practice these estimates have to be generated at the receiver.

However, the number of states to be considered can be reduced significantly, when the cross-coupling is removed, such that the quadrature components of the decoupled channel output $r'(t)$ are only dependent on $s_I(t)$ or $s_Q(t)$, as illustrated in Figure 4 and augmented below:

$$\begin{aligned} r'_I(t) &= s_I(t) * h(t) + n_I(t) \\ &= s_I(t) * h_I(t) + j[s_I(t) * h_Q(t)] + n(t) \\ r'_Q(t) &= -s_Q(t) * h(t) + n_Q(t) \\ &= -\left(s_Q(t) * h_I(t) + j[s_Q(t) * h_Q(t)]\right) + n(t). \end{aligned} \quad (4)$$

This is achieved by generating the estimates $\hat{s}_I(t)$ and $\hat{s}_Q(t)$ of the transmitted signal [8] — using the reliability information output of the decoder — and, as shown in Figure 4, by cancelling the cross-coupling effects of the transmitted quadrature signals from both the I and Q received signal components, namely from $r'_I(t)$ and $r'_Q(t)$, respectively. In the ideal scenario, where perfect signal regeneration is possible, the cross-coupling inherent in the received signal can be successfully removed. Undoubtedly, in practical systems errors will be introduced in the decoupling operation, when inaccurate symbol estimates are regenerated. However, as seen in Section V, the imperfect decoupling effects are compensated with the advent of successive turbo equalization iterations and the performance approaches that of the turbo equalizer utilising the conventional trellis-based equalizer.

After decoupling, the modified complex channel outputs, namely $r'_I(t)$ and $r'_Q(t)$, respectively, can be viewed as the result of convolving both quadrature components independently with the complex CIR on each quadrature arm. Consequently, we can equalise $s_I(t)$ and $s_Q(t)$ independently, hence reducing the number of states in the trellis significantly. Note that in Equation 4 we have assumed that perfect signal regeneration and perfect decoupling is achieved at the receiver, in order to highlight the underlying principle of the reduced complexity equalizer.

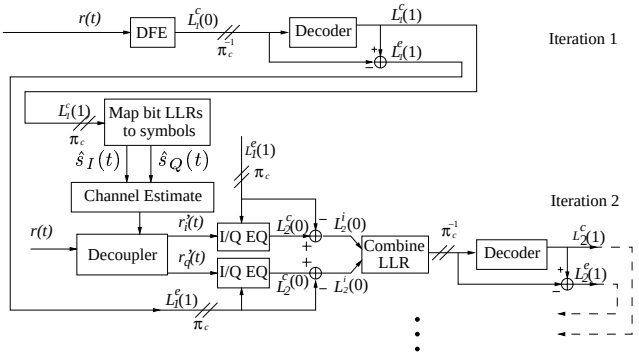

Fig. 5. Schematic of the turbo equalizer employing a DFE and a SISO channel decoder in the first turbo equalization iteration. In subsequent iterations, two I/Q-EQs and one SISO channel decoder is employed. The notation π_c represents a channel interleaver, while π_c^{-1} is used to denote a channel deinterleaver.

IV. OVERVIEW OF THE REDUCED-COMPLEXITY TURBO EQUALIZER

Figure 5 illustrates the schematic of the turbo equalizer utilising two reduced complexity I/Q-EQs. Since the Log-MAP algorithm [16] is employed in the I/Q-EQ and in the channel decoder, the soft decisions generated are in the form of Log-Likelihood Ratios (LLRs). Here, the LLR values of the equalizer and decoder are expressed using vector notations, according to the approach of [7], but using different specific notations. The superscript represents the nature of the LLR, namely 'c' is used for the composite *a posteriori* [17] information, 'i' [17] for the combined channel and extrinsic information and 'e' [17] for the extrinsic information. Furthermore, the subscripts in Figure 5 are used to denote the iteration index, while the argument within the brackets ( ) indicates the index of the receiver stage, where the equalizers are denoted as stage 0, while the channel decoder as stage 1.

At the receiver, the CIR was iteratively estimated using the LMS algorithm [11] and the training symbols of the transmission burst are shown in Figure 3. The initial step-size of the LMS algorithm was set to 0.05. This initial CIR estimate was then utilised during the first turbo equalization iteration by the conventional Decision Feedback Equalizer (DFE) using 15 feedforward taps and 4 feedback taps, as seen in Figure 5. More specifically, in the first turbo equalization iteration, the DFE was employed, since it was capable of providing initial estimates of the transmitted symbols at a low complexity, as compared to the more complex CT-EQ. Subsequently, the Soft-In/Soft-Out (SISO) channel decoder of Figure 5 generates the *a posteriori* LLR $L_1^c(1)$ and then the extrinsic information of the encoded bits, namely

$L_1^e(1)$ is extracted.

In the next iteration, the *a posteriori* LLR $L_1^c(1)$ is used to regenerate estimates of the I and Q components of the transmitted signal, namely $\hat{s}_I(t)$ and $\hat{s}_Q(t)$, as seen in the 'MAP bit LLRs to symbols' block of Figure 5. Since the *a posteriori* information contains information of the transmitted coded bits, it can be used to estimate the modulated symbols [8]. At this stage, the CIR is re-estimated and refined with a smaller step-size of 0.01 using the regenerated symbols of the entire transmission burst. The estimated transmitted quadrature components $\hat{s}_I(t)$ and $\hat{s}_Q(t)$ are then convolved with the estimate of the CIR $h(t)$. Subsequently, at the decoupler block of Figure 5, the resultant signal is used to remove the cross-coupling effect according to Equation 4 from both quadrature components of the transmitted signal, yielding $r'_I(t)$ and $r'_Q(t)$.

After the decoupling operation, $r'_I(t)$ and $r'_Q(t)$ are passed to the I/Q-EQ using the Log-MAP algorithm in the schematic of Figure 5. The I/Q-EQ processes these received quadrature signals and the *a priori* information, which is constituted by the extrinsic LLRs $L_1^e(1)$ of the previous iteration, in order to generate the *a posteriori* information $L_2^c(0)$. Subsequently, the combined channel and extrinsic information $L_2^i(0)$ is extracted from both I/Q-EQs in Figure 5 and combined, before being passed to the Log-MAP channel decoder. As in the first turbo equalization iteration, the *a posteriori* and extrinsic information of the encoded bits, namely $L_2^c(1)$ and $L_2^e(1)$, respectively, are evaluated. The following turbo equalization iterations also obey the same sequence of operations, until the iteration termination criterion is met. In our investigations, the turbo equalization iterations are performed until no further BER performance improvement is obtained.

V. PERFORMANCE OF AQAM SYSTEM

In this section, we will analyse the BER and BPS performance of the turbo-equalized half-rate, K=5 RSC-coded AQAM system. In this joint scheme, the switching thresholds, f_n of Equation 3 were chosen in order to achieve a target BER of approximately 0.01%. The switching thresholds were set as follows: $f_1 = -1.5$dB, $f_2 = 2.5$dB, $f_3 = 6.5$dB and $f_4 = 10.5$dB. Finally, the iterative LMS CIR estimator was also implemented, in order to construct a practical turbo-equalized AQAM system.

The BER and BPS performance of the amalgamated scheme is shown in Figures 6 and 7, respectively. In Figure 6 the AQAM performance was shown, where the iterative CIR estimator was employed and 13 turbo equalization iterations were utilized. Referring to Figure 6, the approximate target BER of 0.01% was achieved and maintained after ten iterations. The BPS throughput performance shown in Figure 7 highlighted the beneficial effect of the AQAM switching mechanism, where the higher order AQAM modes were activated more frequently due to the improving channel quality. Consequently, the BPS throughput improved as the channel SNR increased. The performance of the fixed modulation schemes was also compared

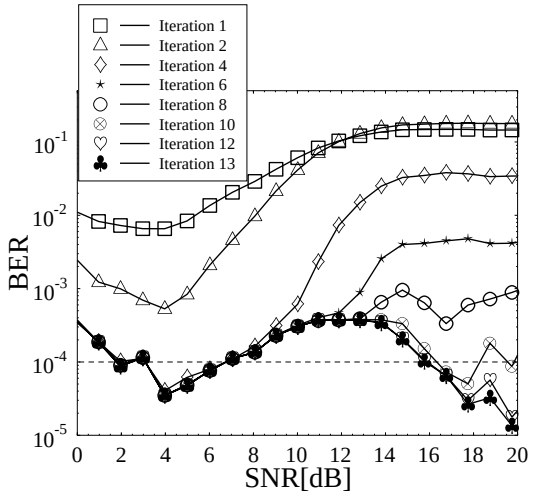

Fig. 6. **BER** performance of the joint **AQAM** and turbo equalization scheme over the three-path, equal-weight, and symbol-spaced fading channel using imperfect CIR estimation, turbo equalization after thirteen iterations and the transmission burst structure of Figure 3.

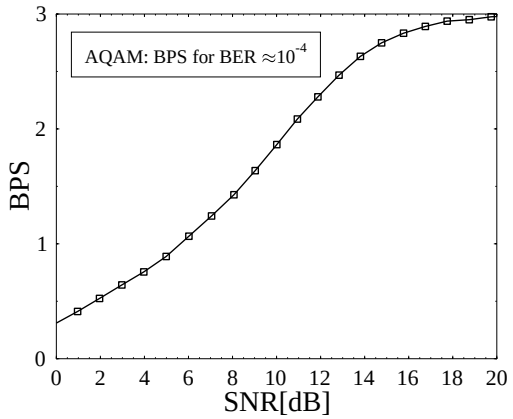

Fig. 7. **BPS** performance of the joint **AQAM** and turbo equalization scheme over the three-path, equal-weight, and symbol-spaced fading channel using imperfect channel estimation, turbo equalization after four iterations and the transmission burst structure of Figure 3.

to that of AQAM in terms of the channel SNR required, in order to achieve a certain BPS throughput for a target BER of approximately 0.01%. The results were compiled and tabulated in Table I. An SNR gain of approximately 1.0dB to 1.5dB was recorded for the AQAM scheme at an effective BPS of 0.5, 1.0 and 2.0, corresponding to the half-rate, K=5 RSC-coded throughput of fixed-mode turbo-equalized BPSK, 4-QAM and 16-QAM over the equal-weight, three-path and symbol-spaced channel, respectively.

VI. CONCLUSIONS

In this contribution, we have introduced a practical AQAM system, which utilized a reduced-complexity turbo equalizer at the receiver. By employing the reduced-complexity TEQ-IQ scheme, higher order modulation

BPS	Channel SNR to achieve BER$\approx 10^{-4}$		AQAM Gain
	Fixed Modulation	AQAM	
0.5	2.8 dB	1.5 dB	1.3 dB
1.0	6.5 dB	5.5 dB	1.0 dB
2.0	12.0 dB	10.5 dB	1.5 dB

TABLE I

THE APPROXIMATE CHANNEL SNRS REQUIRED, IN ORDER TO ACHIEVE AN APPROXIMATE BER OF 0.01% FOR BITS PER SYMBOL (BPS) THROUGHPUT OF **0.5**, **1.0** AND **2.0** FOR THE FIXED MODULATION MODE SYSTEM AND THE AMALGAMATED AQAM AND TURBO EQUALIZATION SYSTEM OVER THE EQUAL-WEIGHT, THREE-PATH AND SYMBOL-SPACED CHANNEL.

modes such as 64-QAM can be utilised, in order to increase the throughput of the system. It was observed that the BPS throughput of the AQAM scheme exhibited SNR gains of approximately 1.0dB to 1.5dB over the equal-weight, three-path and symbol-spaced channel, when compared to the half-rate RSC-coded turbo-equalized BPSK, 4-QAM, 16-QAM and 64-QAM fixed modulation benchmarkers at the effective throughput values of 0.5, 1.0, 2.0 and 3.0 BPS.

Acknowledgement

This work has been funded in the framework of the IST project IST-1999-12070 TRUST, which is partly funded by the European Union. The authors would like to acknowledge the contributions of their colleagues.

VII. REFERENCES

[1] W. Webb and R. Steele, "Variable rate QAM for mobile radio," *IEEE Transactions on Communications*, vol. 43, pp. 2223–2230, July 1995.

[2] S. Sampei, S. Komaki, and N. Morinaga, "Adaptive Modulation/TDMA scheme for large capacity personal multimedia communications systems," *IEICE Transactions on Communications*, pp. 1096–1103, September 1994. .

[3] A. Goldsmith and S. G. Chua, "Variable rate variable power MQAM for fading channels," *IEEE Transactions on Communications*, vol. 45, pp. 1218–1230, October 1997.

[4] C. H. Wong, B. L. Yeap, and L. Hanzo, "Wideband burst-by-burst adaptive modulation with turbo equalization and iterative channel estimation," in *Proceedings of the IEEE Vehicular Technology Conference 2000*, (Tokyo, Japan), pp. 2044–2048, 15-18 May 2000.

[5] C. Douillard, A. Picart, M. Jézéquel, P. Didier, C. Berrou, and A. Glavieux, "Iterative correction of intersymbol interference: Turbo-equalization," *European Transactions on Communications*, vol. 6, pp. 507–511, September-October 1995.

[6] A. Knickenberg, B. L. Yeap, J. Hàmorskỳ, M. Breiling, and L. Hanzo, "Non-iterative Joint Channel Equalisation and Channel Decoding," *IEE Electronics Letters*, vol. 35, pp. 1628–1630, 16 September 1999.

[7] M. J. Gertsman and J. L. Lodge, "Symbol-by-symbol MAP demodulation of CPM and PSK signals on Rayleigh flat-fading channels," *IEEE Transactions on Communications*, vol. 45, pp. 788–799, July 1997.

[8] A. Glavieux, C. Laot, and J. Labat, "Turbo equalization over a frequency selective channel," in *Proceedings of the International Symposium on Turbo Codes & Related Topics*, (Brest, France), pp. 96–102, 3-5 September 1997.

[9] B. L. Yeap, C. H. Wong, and L. Hanzo, "Reduced complexity in-phase/quadrature-phase turbo equalisation with iterative channel estimation," in *IEEE International Communications Conference*, (Helsinki, Finland), 11 - 14 June 2001.

[10] M. S. Yee, B. L. Yeap, and L. Hanzo, "Iterative Radial Basis Function Assisted Turbo Equalisation," in *Proceedings of the IEEE Vehicular Technology Conference 2000*, (Tokyo, Japan), pp. 640–644, 15-18 May 2000.

[11] L. Hanzo, W. Webb, and T. Keller, *Single and Multicarrier Quadrature Amplitude Modulation*. John-Wiley-IEEE Press, 2000.

[12] J. Torrance and L. Hanzo, "Demodulation level selection in adaptive modulation," *Electronics Letters*, vol. 32, pp. 1751–1752, 12 September 1996.

[13] B. Choi and L. Hanzo, "Rake receiver detection of adaptive modulation aided cdma over frequency selective channels," in *Proceedings of the Vehicular Technology Conference 2001*, (Atlantic City, USA), 7-11 October 2001.

[14] B. Choi, M. Münster, L. Yang, and L. Hanzo, "Performance of rake receiver assisted adaptive-modulation based cdma over frequency selective slow rayleigh fading channels," *Electronics Letters*, vol. 19, pp. 247–248, 15 February 2001.

[15] A. Klein, R. Pirhonen, J. Sköld, and R. Suoranta, "FRAMES Multiple Access Mode1 - Wideband TDMA with and without spreading," in *Proceedings of the IEEE International Symposium on Personal, Indoor and Mobile Radio Communications 1997*, (Helsinki, Finland), pp. 37–41, 1-4 September 1997.

[16] P. Robertson, E. Villebrun, and P. Hoeher, "A Comparison of Optimal and Sub-Optimal MAP Decoding Algorithms Operating in the Log Domain," in *Proceedings of the International Conference on Communications*, (Seattle, United States), pp. 1009–1013, 18-22 June 1995.

[17] L. R. Bahl, J. Cocke, F. Jelinek, and J. Raviv, "Optimal Decoding of Linear Codes for Minimising Symbol Error Rate," *IEEE Transactions on Information Theory*, pp. 284–287, March 1974.